



Publication Year	2015
Acceptance in OA @INAF	2020-04-16T15:37:40Z
Title	Radio Timing and Optical Photometry of the Black Widow System PSR J1953+1846A in the Globular Cluster M71
Authors	Cadelano, M.; Pallanca, C.; Ferraro, F. R.; Stairs, I.; Ransom, S. M.; et al.
DOI	10.1088/0004-637X/807/1/91
Handle	http://hdl.handle.net/20.500.12386/24078
Journal	THE ASTROPHYSICAL JOURNAL
Number	807

RADIO TIMING AND OPTICAL PHOTOMETRY OF THE BLACK WIDOW SYSTEM PSR J1953+1846A IN THE GLOBULAR CLUSTER M71*

M. CADELANO^{1,2}, C. PALLANCA¹, F. R. FERRARO¹, I. STAIRS³, S. M. RANSOM⁴, E. DALESSANDRO¹, B. LANZONI¹,
J. W. T. HESSELS^{5,6}, AND P. C. C. FREIRE⁷

¹ Dipartimento di Fisica e Astronomia, Università di Bologna, Viale Bertini Pichat 6/2, I-40127 Bologna, Italy

² INAF—Osservatorio Astronomico di Bologna, via Ranzani 1, I-40127 Bologna, Italy

³ Department of Physics and Astronomy, University of British Columbia, 6224 Agricultural Road, Vancouver, BC V6T1Z1, Canada

⁴ National Radio Astronomy Observatory (NRAO), 520 Edgemont Road, Charlottesville, VA 22901, USA

⁵ ASTRON, The Netherlands Institute for Radio Astronomy, Postbus 2, 7990 AA, Dwingeloo, The Netherlands

⁶ Anton Pannekoek Institute for Astronomy, University of Amsterdam, Science Park 904, 1098 XH Amsterdam, The Netherlands

⁷ Max-Planck-Institute für Radioastronomie, D-53121 Bonn, Germany

Received 2015 March 24; accepted 2015 May 13; published 2015 July 2

ABSTRACT

We report on the determination of the astrometric, spin, and orbital parameters for PSR J1953+1846 A, a “black widow” binary millisecond pulsar in the globular cluster M71. By using the accurate position and orbital parameters obtained from radio timing, we identified the optical companion in Advanced Camera for Surveys/*Hubble Space Telescope* images. It turns out to be a faint ($m_{F606W} \gtrsim 24$, $m_{F814W} \gtrsim 23$) and variable star located at only $\sim 0''.06$ from the pulsar timing position. The light curve shows a maximum at the pulsar inferior conjunction and a minimum at the pulsar superior conjunction, thus confirming the association with the system. The shape of the optical modulation suggests that the companion star is heated, likely by the pulsar wind. The comparison with the X-ray light curve possibly suggests the presence of an intra-binary shock due to the interaction between the pulsar wind and the material released by the companion. This is the second identification (after COM-M5C) of an optical companion to a black widow pulsar in a globular cluster. Interestingly, the two companions show a similar light curve and share the same position in the color–magnitude diagram.

Key words: globular clusters: individual (M71, NGC 6838) – pulsars: individual (PSR J1953+1846A) – techniques: photometric – time

1. INTRODUCTION

Millisecond pulsars (MSPs) are rapidly spinning neutron stars (NSs), formed in a binary system where, according to the canonical scenario (Alpar et al. 1982; Bhattacharya & van den Heuvel 1991), a slowly rotating NS is spun up through mass accretion from an evolving companion star. The accretion phenomena are usually observed during the phases of low-mass X-ray binaries (LMXBs), which can be considered the progenitors of MSPs. The process usually leads to a deep transformation of both the accreting and the donor stars: the former is accelerated to millisecond spin periods, while the latter can evolve into an intermediate anomalous evolutionary phase (see, e.g., MSP-A in NGC 6397; Ferraro et al. 2001a), before reaching the final stage of a (possibly He) white dwarf (WD; e.g., MSP-A in NGC 6752; Ferraro et al. 2003a).

Although the Galaxy is ~ 100 times more massive than the entire Galactic globular cluster (GC) ecosystem, about 40% of the known MSP population is found in GCs. Such an overabundance is indicative of a strongly enhanced dynamical activity in these dense stellar systems. In fact, in the Galactic field the most plausible channel for the formation of MSPs is the evolution of primordial binaries, while in GCs dynamical interactions promote the formation of a conspicuous number of exotic objects, such as blue straggler stars, X-ray binaries, cataclysmic variables, and MSPs (Bailyn 1992; Cool et al. 1995; Ferraro et al. 1995, 2001b; Pooley et al. 2003; Ransom et al. 2005a), which can be used to trace the complex

interplay between dynamics and stellar evolution (e.g., Goodman & Hut 1989; Hut et al. 1992; Phinney 1992; Ferraro et al. 1995, 2003b, 2009, 2012; Possenti et al. 2003). Thus, especially in the very center of these systems, we expect to find a large number of NSs which are (or have been) affected by dynamical processes such as tidal captures or exchange interactions (see e.g., Ivanova et al. 2008). In this respect, the study of optical companions to binary MSPs in GCs is of utmost importance since it opens the possibility of evaluating the frequency and timescales of dynamical interactions in dense stellar systems, to explore the impact of dynamics on MSP evolutionary paths, and to investigate stellar evolution under extreme conditions (see e.g., Ferraro et al. 2003c; Sabbi et al. 2003a, 2003b; Mucciarelli et al. 2013).

Although the majority of binary MSPs have low-mass He WD companions, recent PSR searches have considerably increased the number of non-canonical binary MSPs. Among these, “black widows” (BW) and “redbacks” (RB) are of particular interest due to the presence of radio eclipses of the MSP signal, caused by a significant amount of ionized material ablated from the companion star because of the energy injected by the pulsar (PSR; e.g., Ruderman et al. 1989). The eclipsing regions are usually larger than the companion Roche lobes, thus suggesting the presence of a nondegenerate and possibly bloated star, as confirmed by several optical identifications (e.g., Ferraro et al. 2001a; Edmonds et al. 2002; Cocozza et al. 2008; Pallanca et al. 2010, 2013, 2014a). These systems are characterized by small orbital eccentricities, tight orbits (orbital periods $P_{\text{orb}} \lesssim 1$ day) and small mass functions, thus implying the presence of a low-mass companion. Indeed, RB companion stars usually have masses of $\sim 0.1\text{--}0.5 M_{\odot}$, while

* Based on observations collected with the NASA/ESA *HST* (Prop. 12932), obtained at the Space Telescope Science Institute, which is operated by AURA, Inc., under NASA contract NASS-26555.

BW companions are much less massive ($M < 0.1 M_{\odot}$). Such a small value could be due to vaporization from the strong MSP radiation and relativistic wind; thus these systems may provide a possible explanation of the existence of isolated MSPs, even if their observed number is too large if compared to the expected timescale for the total ablation of the companion stars (Eichler & Levinson 1988). The physical mechanism favoring the formation of an RB instead of a BW is not well understood yet. Benvenuto et al. (2014) argued that RBs may evolve into BW systems, as a direct consequence of ablation processes, although this cannot apply to all RBs since some of them could evolve into canonical He WD systems. On the other hand, Chen et al. (2013) suggested that BWs cannot result from the evolution of RBs and that the discriminant factor leading to the formation of an RB instead of a BW is the reprocessing efficiency of the MSP emission by the companion star, likely related to geometrical factors.

Since the first eclipsing MSPs were preferentially found in GCs, it was commonly believed that these systems form exclusively in crowded environments (King et al. 2003), mostly as a consequence of exchange interaction, and the few objects discovered in the Galactic field were born in GCs and later ejected. Indeed, at that time, the ratio between the number of eclipsing MSPs and canonical MSPs was significantly higher in GCs than in the Galactic field. This scenario has been recently altered by the discovery of a large number of eclipsing MSPs in the Galactic field, both in blind surveys (Burgay et al. 2006; Bates et al. 2011; Keith et al. 2012) and especially in surveys aimed at the radio identification of *Fermi* sources (e.g., Keith et al. 2011; Ransom et al. 2011). Hence, these objects can also form in the field from the undisturbed evolution of LMXB systems, with no need for dynamical interactions with other stars. In such a scenario, the fraction of eclipsing to canonical MSPs should be similar in the field and in GCs, irrespective of their interaction rate per binary, since binaries in very tight orbits are unlikely to be disrupted (Verbunt & Freire 2014). As an example, the BWs J1518+0204C and J1807–2459A are located respectively in a GC with a very low interaction rate (M5) and in the one with the largest rate (NGC 6544; Pallanca et al. 2014a; Verbunt & Freire 2014). Still, both the objects appear to be in relatively undisturbed systems (no orbital eccentricity). Understanding the formation of BWs and RBs, including the possible role of stellar interaction, strongly motivates multi-wavelength studies, both in GCs and in the Galactic field.

Despite the importance of MSP optical companions, finding them in crowded stellar systems like GCs is extremely challenging. Only nine companions have been discovered so far in GCs. Three companions are He WDs (see Edmonds et al. 2001; Ferraro et al. 2003a; Sigurdsson et al. 2003), as expected from the canonical formation scenario, five are RB companions (see Ferraro et al. 2001a; Edmonds et al. 2002; Coccozza et al. 2008; Pallanca et al. 2010, 2013) and only one is a BW companion (see Pallanca et al. 2014a). Here we report the radio timing ephemeris of PSR J1953+1846 A (hereafter M71A) in the GC M71 (NGC 6838) and the identification of its companion star.

M71A is the only MSP known so far in M71 (Ransom et al. 2005b). M71 is a low-density GC ($\log \rho_0 = 2.83$ in units of $L_{\odot} \text{pc}^{-3}$; Harris 1996), in a disk-like orbit (Geffert & Maintz 2000), located at ~ 4 kpc from the Earth. It is one of the most metal-rich clusters among halo GCs (Harris 1996) and

its surface brightness profile shows an extended core ($r_c = 37''.8$; Harris 1996) and no signatures of core collapse. M71A was discovered in a targeted survey of all GCs visible with the 305 m Arecibo radio telescope (Hessels et al. 2007). It is located at $\alpha = 19^{\text{h}}53^{\text{m}}46^{\text{s}}.42$; $\delta = 18^{\circ}47'04''.84$, at a projected distance of only $20''$ (0.53 core radii) from the cluster center (Goldsbury et al. 2010), and it has a spin period of ~ 4.9 ms and a low eccentricity orbit of ~ 4.2 hr. M71A is classified as a BW. In fact, because of its very low mass function ($f = 1.6 \cdot 10^{-5} M_{\odot}$), the companion is expected to have a minimum mass of $\sim 0.032 M_{\odot}$. Moreover, as commonly found for BW systems, the radio signal shows eclipses for about 20% of the orbital period (at 1400 MHz observing frequency), likely due to material stripped from an evaporating companion. A *Chandra* X-ray observation of this cluster revealed a source in a position compatible with the PSR location and a luminosity of about $10^{31} \text{ erg s}^{-1}$ in the spectral range 0.3–8.0 keV (Elsner et al. 2008). The light curve is consistent with a non-steady source and the photon index ($\Gamma = 1.89 \pm 0.32$) suggests magnetospheric radiation and/or an emission from intra-binary shocks. In the context of an optical study of the M71 X-ray sources, Huang et al. (2010) suggested as possible optical companion to M71A a star located at $\sim 0''.1$ from the radio PSR and lying along the red side of the cluster main sequence (MS), in a region commonly occupied by binary systems. Nonetheless, its absolute magnitude ($M_V \sim 8.5$) implies a mass of about $0.5 M_{\odot}$, inconsistent with the radio-derived mass function (in fact such a large mass would be compatible only with a nearly face-on orbit, where no radio eclipses are expected). Hence, Huang et al. (2010) concluded that this object is unlikely to be the real companion, which could be still below the detection threshold or, alternatively, that M71A could be a hierarchical triple system.

In Section 2 the radio timing analysis is presented, while Section 3 is devoted to the optical identification of the companion star. In Section 4 we discuss the results and in Section 5 we summarize the current knowledge about this BW system.

2. RADIO TIMING

Timing observations were carried out with the 305 m William E. Gordon telescope at the Arecibo Observatory in Puerto Rico, between MJDs 52420 (2002 May 26) and 53542 (2005 June 21), with the initial discovery observations on MJD 52082 (2001 June 22) incorporated into the timing solution. The Gregorian L-band Wide receiver was used for the observations, sending dual-polarization data to the Wideband Arecibo Pulsar Processor (WAPP; see Dowd et al. 2000) autocorrelation spectrometers. For most of the timing observations, three WAPPs were used, at frequencies centered near 1170, 1420, and 1520 MHz, although in the beginning, and occasionally thereafter, only one WAPP was used, and sometimes four WAPPs were used. The WAPPs were configured to autocorrelate three-level samples with 256 lags and accumulate these for $64 \mu\text{s}$, then sum polarizations and write the results to disk as 16 bit numbers. See Hessels et al. (2007) for details of the observations.

Offline, the PRESTO software⁸ was used to partially dedisperse the data into 32 subbands, to reduce the data size while still facilitating searches for further PSRs in the cluster

⁸ github.com/scottransom/presto

Table 1
Timing Parameters for PSR J1953+1847 (M71A)^a

Parameter	Value
Measured Parameters	
R.A., α (J2000)	19 ^h 53 ^m 46 ^s .41966(3)
Decl., δ (J2000)	+18° 47' 04" 8472(7)
Spin frequency F , Hz	204.57006473073(3)
Spin frequency derivative, \dot{F} (10^{-15}) (s^{-2})	-2.0299(3)
Spin frequency second derivative, \ddot{F} (10^{-25}) (s^{-3})	5.4(3)
Epoch (MJD)	52812.0
Dispersion measure, DM (cm^{-3} pc)	117.3941(15)
DM derivative (cm^{-3} pc yr ⁻¹)	-0.0274(17)
Orbital period, P_b (days)	0.1767950297(2)
Projected semimajor axis, x (s)	0.0782246(12)
Epoch of ascending node, T_0 (MJD)	52811.8761877(3)
Derived Parameters	
Spin period, P (ms)	4.8883007458412(6)
Spin period derivative \dot{P} (10^{-20})	4.8506(8)
Spin period second derivative \ddot{P} (10^{-29}) (s^{-1})	-1.28(7)
Angular offset from cluster center θ_{\perp} (arcmin)	0.33
Intrinsic period derivative \dot{P}_{int} (10^{-20})	$4.3 < \dot{P}_{\text{int}} < 5.4$
Characteristic age τ_c (Gyr)	$1.4 < \tau_c < 1.8$
Surface magnetic field B_0 (10^8) (G)	$4.6 < B_0 < 5.2$
Mass function f (M_{\odot})	0.0000164427(8)
Minimum companion mass m_c (M_{\odot}) ^b	0.032

Notes.

^a Numbers in parentheses are uncertainties in the last digits quoted.

^b Computed assuming an orbital inclination angle of 90° and a pulsar mass of $1.4 M_{\odot}$.

(no additional radio PSRs were found, despite careful searches of the majority of the acquired timing data). The subbands were then folded modulo the best-known PSR ephemeris. A Gaussian profile was fit to the summed profile from several observations for use as a standard profile, and the FFTFIT algorithm (Taylor 1992) was used to determine pulse times of arrival (TOAs). Time segments corresponding to eclipses and to the times when M71 transited at Arecibo (during which the telescope could not track the cluster) were not considered in the timing analysis.

Timing analysis was performed with the TEMPO software package⁹ using the DE421 Solar System ephemeris and the TT (BIPM) clock standard. The BT timing model of Blandford & Teukolsky (1976) was used, as the orbit has no significant eccentricity. The timing parameters are listed in Table 1 and residuals are presented in Figure 1. The rms postfit residual is $35 \mu\text{s}$. The reduced- χ^2 of the fit is 4.8; however, we list the parameter uncertainties as reported by TEMPO without scaling, as the epoch-to-epoch wander in the residuals is likely due to the interactions between the two stars (see Figure 2) rather than to any misestimation of the TOA uncertainties. The high-precision radio timing position is slightly offset ($0''.06$) from the position of the optical counterpart (see Section 3), but agrees within the much larger uncertainty ($0''.2$) of the latter. Following the reasoning in Freire et al. (2005), we find the maximum possible acceleration due to the gravitational field of the cluster for this line of sight to be $\pm 3.2 \times 10^{-10} \text{ m s}^{-2}$. This

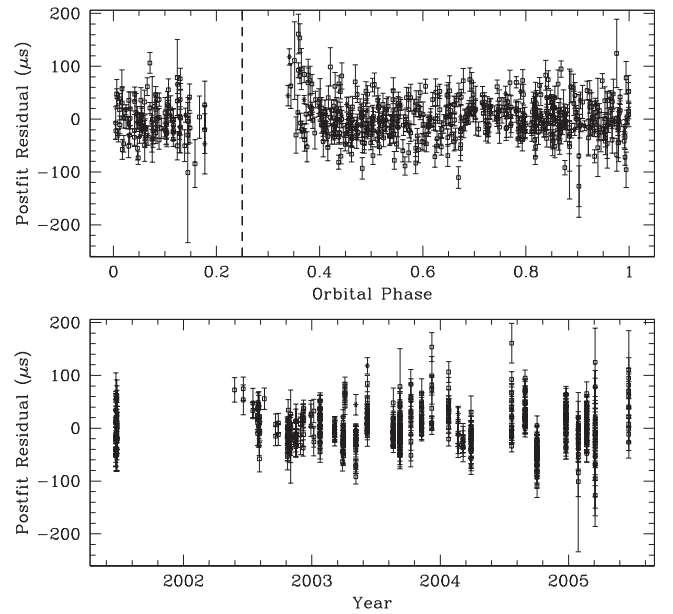


Figure 1. Postfit timing residuals for M71A, as functions of orbital phase and date. The dashed line indicates orbital phase 0.25, the PSR superior conjunction. The asymmetric eclipse spans just over 15% of the orbit, which is typical for BW systems at radio frequencies below ~ 2 GHz (e.g., Fruchter et al. 1988).

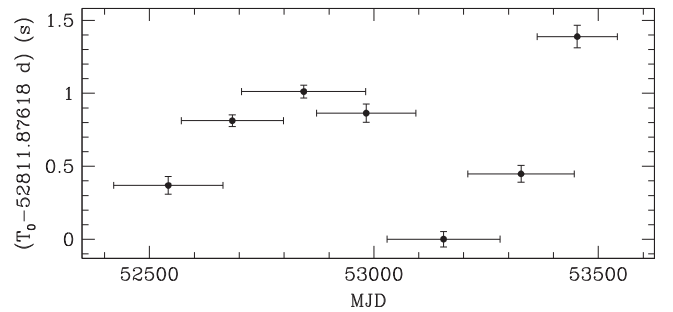


Figure 2. Variation of the time of passage through ascending node (orbital phase 0), computed for overlapping segments of data and holding all other timing parameters fixed at their nominal values.

implies that most of the observed pulse period derivative (\dot{P}) is intrinsic. Further corrections due to the differential acceleration in the Galaxy (e.g., Nice & Taylor 1995; Reid et al. 2014) are small. Given the small velocity dispersion in the core of the cluster (2.3 km s^{-1} ; Harris 1996), the velocity of the PSR relative to that of the cluster should be very small; therefore its proper motion should be very similar to the proper motion of the cluster as a whole. A recent measurement of the proper motion of the cluster amounts to 3.93 mas yr^{-1} (Kharchenko et al. 2013), making the corresponding correction to \dot{P} (Shklovskii 1970) about half the size of that due to the Galactic acceleration. The timing data do not allow us to derive a reliable proper motion for the PSR. We use the range of allowed accelerations to constrain the intrinsic \dot{P} as well as the characteristic age and surface magnetic field in Table 1.

The PSR is asymmetrically eclipsed between approximate orbital phases of 0.18 and 0.35, where orbital phase 0.25 represents superior conjunction. The eclipses begin fairly abruptly, but when the signal returns it at first suffers excess dispersive delay due to ionized material within the orbit (Figure 3). A discussion of the companion size and inclination

⁹ tempo.sourceforge.net

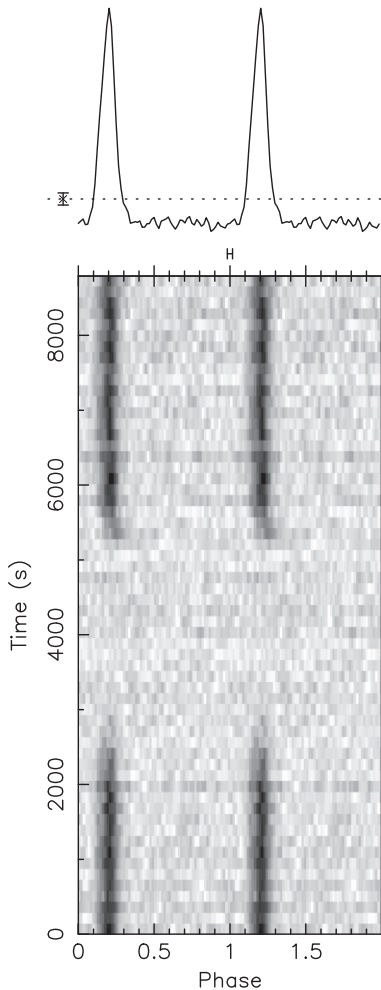


Figure 3. Observation of M71A on MJD 52798 (2003 June 8), using three WAPPs to cover 300 MHz of contiguous bandwidth. The abrupt disappearance of the PSR at the start of eclipse, as well as the slight dispersive delay on reappearance, are clearly visible. The cumulative pulse profile is plotted twice at the top of the figure.

angle is presented in Section 4. The mass loss from the companion star has a further manifestation in the variation of orbital parameters: Figure 2 shows the value of the time of ascending node passage for overlapping subsets of the data. The variation is comparable to that seen in other BW eclipsing systems (e.g., Arzoumanian et al. 1994; Ng et al. 2014) and significantly less than what is typically present in the RB systems (e.g., Archibald et al. 2013), which have much more massive, likely nondegenerate companion stars.

3. OPTICAL PHOTOMETRY OF THE COMPANION STAR

3.1. Observations and Data Analysis

The identification of the companion to M71A has been performed through two data sets of high-resolution images acquired with the Wide Field Camera (WFC) of the Advanced Camera for Surveys (ACS) mounted on the *Hubble Space Telescope* (*HST*). The primary data set has been obtained on 2013 August 20 (GO12932, P.I.: Ferraro) and consists of a set of ten images in the F606W filter (with exposure times: 2×459 s; 3×466 s; 5×500 s) and nine images in the F814W filter (5×337 s; 3×357 s; 1×440 s). We also analyzed an archival data set, obtained on 2006 July 1

(GO1775, P.I.: Sarajedini) with the same instrument and same filters. It consists of four F606W images with an exposure time of 75 s and four F814W images with an exposure time of 80 s.

The standard photometric analysis (see Dalessandro et al. 2008a, 2008b) has been performed on the “flc” images, which are corrected for flat field, bias, dark counts, and charge transfer efficiency. These images have been further corrected for “Pixel-Area-Map”¹⁰ with standard IRAF procedures. By using the DAOPHOT II ALLSTAR and ALLFRAME packages (Stetson 1987), we performed an accurate photometric analysis of each image. First of all, we modeled the point-spread function (PSF) by using a sample of ~ 200 bright but not saturated stars. The model has been chosen on the basis of a χ^2 test and, in every image, the best fit is provided by a Moffat function (Moffat 1969). Then we performed a source detection analysis, setting a 3σ detection limit, where σ is the standard deviation of the measured background. Once a list of stars was obtained, we performed a PSF-fitting in each image. In the resulting catalog we included only stars present at least in half the images for each filter. For each star, we homogenized the magnitudes estimated in different images, and their weighted mean and standard deviation have been finally adopted as the star mean magnitude and its related photometric error (see Ferraro et al. 1991, 1992). However, in order to perform variability studies, for each source we also kept the homogenized magnitude measured in each frame in both filters. Then, instrumental magnitudes have been calibrated to the VEGAMAG system, cross-correlating¹¹ our catalog with that by Anderson et al. (2008), using the ~ 7600 stars in common.

Since the WFC images suffer heavily from geometric distortion, we corrected the instrumental positions (x , y) by applying the equations reported by Meurer et al. (2003) and using the coefficients in Hack & Cox (2001). Then we transformed instrumental positions into the absolute astrometric system (α , δ) using the stars in common with the Anderson et al. (2008) catalog. The resulting astrometric solution has an accuracy of $\sim 0''.14$ in α and of $\sim 0''.13$ in δ , corresponding to a total position accuracy of $\sim 0''.2$.

3.2. The Companion to M71A

The search for the companion star to M71A was performed by means of an accurate photometric analysis of all the detectable objects within a $5'' \times 5''$ wide region centered on the nominal position of the MSP. Figure 4 shows the zoomed ($0''.5 \times 0''.5$) central part of that region. As can be seen, a relatively bright object is found to have a position compatible with the X-ray source (dashed circle) and the radio source (solid-line circle). This is the star proposed by Huang et al. (2010) to be the optical counterpart to M71A. However, a much fainter object, showing a strong variability, is visible in the figure. This is a quite promising object and it is located at $\alpha = 19^{\text{h}}53^{\text{m}}46^{\text{s}}.4062$; $\delta = 18^{\circ}47'04''.793$, only $0''.06$ from the radio position and $0''.13$ from the X-ray source, thus in perfect positional coincidence within our positional uncertainty ($\sim 0''.2$). In the primary data set, it has been detected in nine (out of ten) images in the F606W filter, with a magnitude

¹⁰ For more details see the ACS Data Handbook.

¹¹ We used CataXcorr, a code that is specifically developed to perform accurate astrometric solutions. It has been developed by P. Montegriffo at INAF-Osservatorio Astronomico di Bologna. This package is available at <http://davide2.bo.astro.it/~paolo/Main/CataPack.html>, and has been successfully used in a large number of papers by our group in the past ten years.

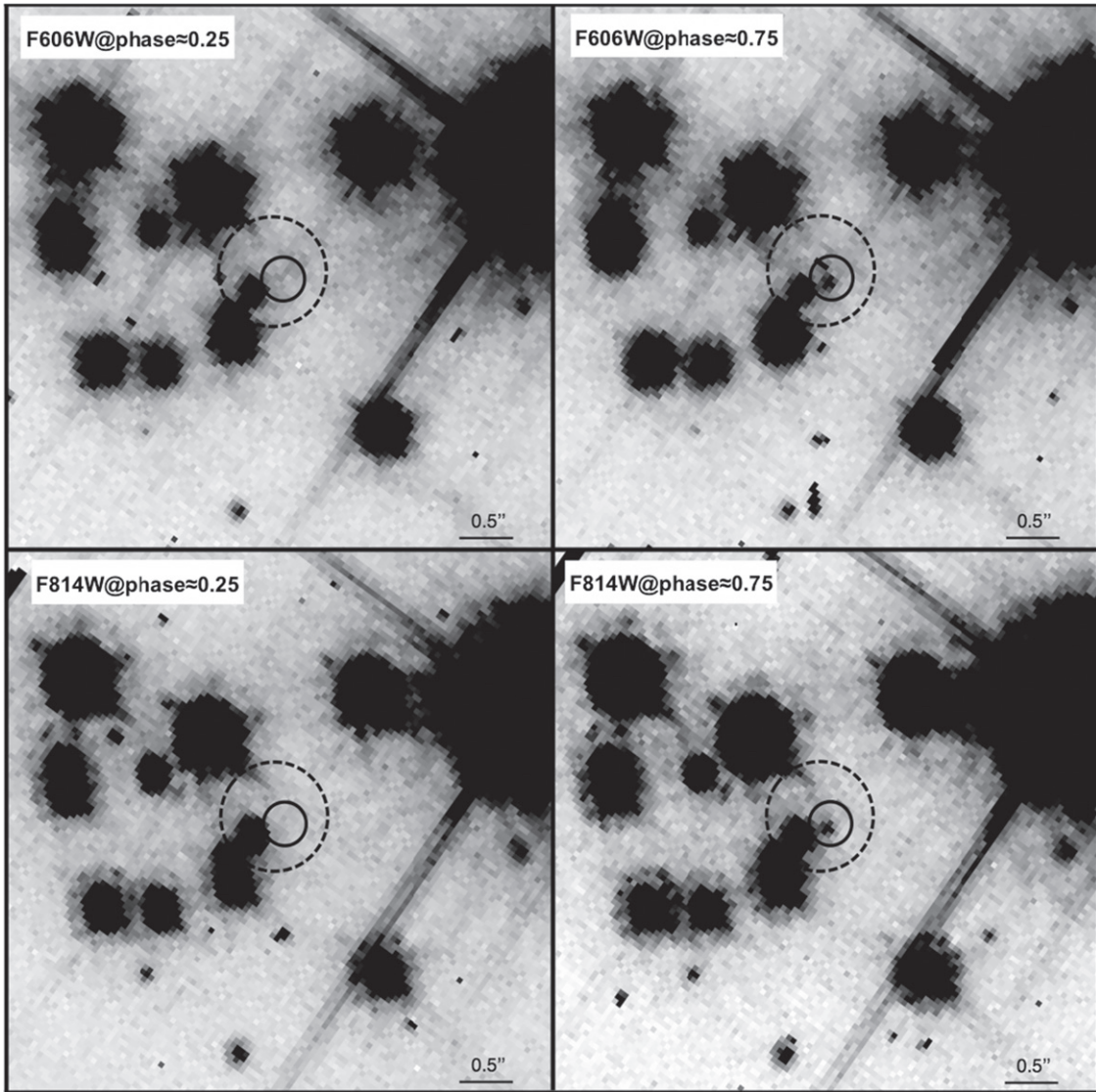


Figure 4. Primary data set *HST* images of the $5'' \times 5''$ region around the nominal position of M71A. The filters and the orbital phases are labeled in each panel. The solid circle is centered on the radio position and it has a radius of $0.2''$ (which is larger than the formal uncertainty from PSR timing). The dashed circle is centered on the X-ray counterpart and it has a radius of $0.5''$. The relatively bright star on the left border of the solid circle is the candidate optical companion proposed by Huang et al. (2010). COM-M71A is clearly visible inside the solid circle in the right panels (corresponding to the inferior conjunction of the PSR, where the companion reaches maximum brightness), while in the left panels (at superior conjunction of the PSR) it is below the detection threshold.

variation ranging from $m_{F606W} \approx 24.3$ to $m_{F606W} \approx 27$, while in the F814W filter has been detected in six images (out of nine) and the magnitude varies from $m_{F814W} \approx 23.4$ to $m_{F814W} \approx 24.9$. Unfortunately, the images in the archival data set are too shallow to properly detect this faint object: in fact it turned out to be above the detection threshold in only one exposure in the F814W filter. For the four deep exposures of the primary data set in which the star is not visible, we estimated an upper magnitude limit by simulating an artificial star of decreasing magnitude at the position of the candidate companion. The derived detection threshold turned out to be $m_{F606W} \sim 26.5$ and $m_{F814W} \sim 25.9$.

In order to reliably establish that the detected star is the binary companion to M71A, we built the light curve in both the available filters by folding the optical measurements with the orbital period and the ascending node time of the PSR (see Table 1). The results are shown in Figure 5, and in Table 2 we report the MJD of the images with their related orbital phases

and magnitudes. As can be seen, the light curves show a sinusoidal modulation spanning at least three magnitudes and it is fully consistent with the orbital period of the binary system. This establishes the physical connection between the variable star and the MSP. Indeed the exposures in which the star is not detected correspond nicely to the light-curve minima. The curves have a maximum at $\phi \approx 0.75$, corresponding to the PSR inferior conjunction (where we observe the companion side facing the PSR) and a minimum at $\phi \approx 0.25$, corresponding to the PSR superior conjunction (where we observe the back side of the companion). This behavior is indicative of a strong heating of the companion side exposed to the PSR emission and it is in good agreement with the observed optical properties of other similar objects (e.g., Stappers et al. 2001; Reynolds et al. 2007; Pallanca et al. 2012, 2014a; Breton et al. 2013; Li et al. 2014). For the sake of comparison, in Figure 6 we plot the light curve (folded following the same procedure described above) of the possible companion suggested by Huang et al.

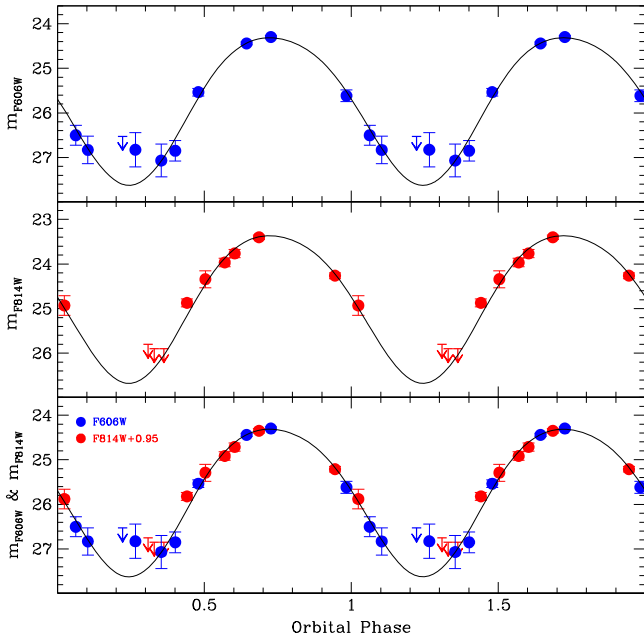


Figure 5. Light curves of COM-M71 A in the F606W and F814W filters separately (upper and middle panels) and for the combination of the two (bottom panel), obtained after a 0.95 mag shift of the F814W magnitudes. All curves are folded with the radio parameters and two periods are shown for clarity. Circles mark the observed points; arrows are the magnitude upper limits for the images where the star is below the detection threshold. The black curve in each panel is the best analytical model obtained from the combined light curve and then adapted to each filter.

Table 2
Optical Observations of COM-M71A

ϕ	t (MJD)	m_{F606W}	m_{F814W}
0.02	56524.57602385	...	24.9 ± 0.2
0.06	56524.58290459	26.5 ± 0.2	...
0.10	56524.59012681	26.8 ± 0.3	...
0.22	56524.43431532	>26.5	...
0.26	56524.44193085	26.8 ± 0.4	...
0.31	56524.44960589	...	>25.9
0.33	56524.63013255	...	>25.9
0.35	56524.45750982	27.1 ± 0.4	...
0.36	56524.63586163	...	>25.8
0.40	56524.64270200	26.8 ± 0.2	...
0.44	56524.64977385	...	24.87 ± 0.09
0.48	56524.65661404	25.54 ± 0.08	...
0.50	53867.78512088 ^a	...	24.3 ± 0.2
0.57	56524.49569959	...	23.97 ± 0.09
0.60	56524.50166033	...	23.76 ± 0.09
0.64	56524.50885348	24.44 ± 0.03	...
0.68	56524.51627848	...	23.40 ± 0.05
0.73	56524.52347163	24.30 ± 0.03	...
0.94	56524.56203070	...	24.26 ± 0.06
0.98	56524.56891144	25.6 ± 0.1	...

Notes. Orbital phases (ϕ), corresponding MJD (t) of the observations, and observed magnitudes or upper limits in both filters.

^a This is the only image of the archival data set where the companion star is above the detection threshold.

(2010). As can be seen, the star does not show any significant flux variation.

All these pieces of evidence suggest that the faint variable (which we name COM-M71A) is the optical companion to the BW M71A. It is the tenth MSP optical companion and the

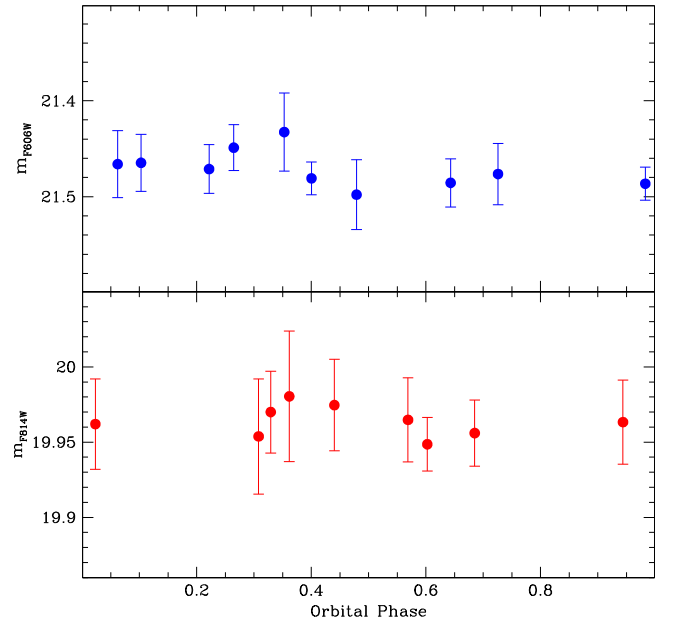


Figure 6. Light curves of the candidate companion proposed by Huang et al. (2010), folded with radio orbital parameters. The absence of any magnitude modulation as a function of the orbital phase is the definitive confirmation that this object is not connected to M71A.

second to a BW system in a GC. In the color–magnitude diagram (CMD), COM-M71A is located at faint magnitudes in a region between the MS and the WD cooling sequences, where no normal GC stars are expected. This position is indicative of a nondegenerate or semi-degenerate, low-mass and swollen star. Interestingly, the position of this object in the CMD is quite similar to that of COM-M5C, the only companion to a BW system known in GCs up to now and recently identified by Pallanca et al. (2014a) in the GC M5.

4. DISCUSSION

Since the available data do not uniformly sample the orbital phases of the system in either the F606W or the F814W filters (see upper and middle panels of Figure 5), in order to accurately determine the light curve of the companion star we combined the two data sets together by applying a 0.95 mag shift to the F814W magnitudes (bottom panel of Figure 5). We then used the software GRATIS¹² and a χ^2 criterion to determine the model with two harmonics¹³ giving the best fit to the curve. This is shown as a solid line in the bottom panel of Figure 5. Finally, we verified that the same solution also provides a good fit to the light curves in each filter separately. Indeed, the reduced χ^2 turned out to be 1.50 for the F606W filter, and 1.75 in F814W (see the solid curves in the upper and middle panels of Figure 5). This demonstrates that no significant modulation of the stellar color (temperature) along the orbit is measurable from the available data set, and a much finer sampling of the light curve is needed to provide additional clues on this possibility. In Table 3 we report the maximum and minimum values for both the magnitude and the flux in each

¹² “Graphical Analyzer for Time Series” is software aimed at studying stellar variability phenomena. It was developed by Paolo Montegriffo at INAF–Osservatorio Astronomico di Bologna.

¹³ Note that a single harmonic model (i.e., a sinusoidal function) does not provide a good match of the observed light curve.

Table 3
Optical Properties of COM-M71A

	F606W	F814W
m_{bright}	24.31 ± 0.01	23.37 ± 0.02
m_{faint}	27.62 ± 0.09	26.7 ± 0.1
$F_{\text{bright}} (10^{-17} \text{ erg cm}^{-2} \text{ s}^{-1})$	126 ± 1	128 ± 2
$F_{\text{faint}} (10^{-17} \text{ erg cm}^{-2} \text{ s}^{-1})$	5.9 ± 0.5	6.1 ± 0.6
$\Delta F (10^{-17} \text{ erg cm}^{-2} \text{ s}^{-1})$	120 ± 50	120 ± 60
$L_{\text{bright}} (10^{29} \text{ erg s}^{-1})$	24.2 ± 0.2	24.5 ± 0.4
$L_{\text{faint}} (10^{29} \text{ erg s}^{-1})$	1.15 ± 0.09	1.2 ± 0.1

Note. Maximum and minimum luminosities of COM-M71A as derived from the model light curve.

filter, evaluated from the best-fit model by following the procedure described in Bohlin (2012) for the ACS. The uncertainties are calculated by using the mean photometric errors for stars with similar magnitudes. The magnitude shift needed to superimpose the F814W light curve on that in the F606W filter implies a color index of 0.95 ± 0.12 for the companion star. By adopting a $0.54 M_{\odot}$ WD cooling sequence from the BaSTI catalog¹⁴ (Manzato et al. 2008; Salaris et al. 2010), this value can be converted into a temperature of 5100 ± 800 K, which is in good agreement with those evaluated for other BW systems (e.g., Stappers et al. 2001; Pallanca et al. 2012, 2014a; Breton et al. 2013; Li et al. 2014).

In Figure 7 we show the CMD, with the shaded rectangle marking the region occupied by COM-M71A during the orbital period. The height of the rectangle corresponds to the maximum m_{F606W} magnitude difference expected from the best-fit model shown in Figure 5, while the width corresponds to the photometric error at the minimum luminosity. As already mentioned, the star is located between the MS and the WD cooling sequence, and it spans a range of about three magnitudes. Of particular interest is the predicted star position during the PSR superior conjunction, where we expect to see the stellar side not exposed to the PSR flux (clearly this is exactly the case only for $i = 90^{\circ}$). The CMD position of COM-M71A in this phase could be compatible with the He WD cooling sequence, suggesting a semi-degenerate stellar structure. However, at these low luminosities, our analytical model is not appropriately constrained by data. Therefore, in order to confirm this possibility, further observations are needed. In principle, the companion mass can be constrained from the comparison of its CMD position and theoretical isochrones. However, in the case of strongly perturbed stars the mass inferred in this way can be overestimated, or suggestive of inclination angles too small to be consistent with the presence of radio eclipses (see Ferraro et al. 2003a; Pallanca et al. 2010; Mucciarelli et al. 2013). In our case, not only is the companion position in the CMD clearly out of the canonical evolutionary sequences, but also its minimum luminosity is not properly constrained by the observations.

Assuming that the companion’s optical emission is mostly due to blackbody radiation, the luminosity and temperature of this star would be consistent with an object of radius $R_{\text{BB}} \leq 0.02 R_{\odot}$. However, the companions to BWs usually suffer from strong tidal distortion due to the interaction with the PSR; therefore they are swollen and possibly they can even fill their Roche lobes. Furthermore, the presence of radio eclipses

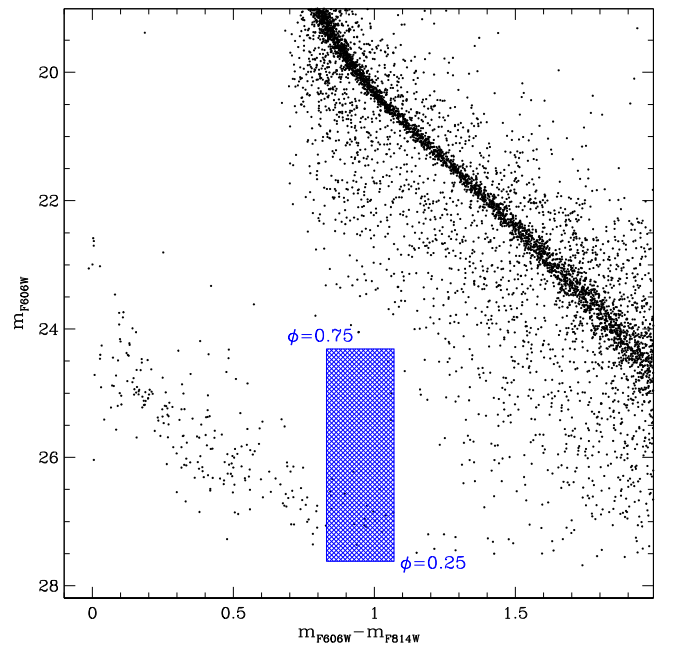


Figure 7. CMD of M71 with highlighted in blue the region occupied by COM-M71A during the whole orbital period, as predicted by the light-curve model (see text, Figure 5, and Table 3).

suggests that the simple R_{BB} is a gross underestimate of the true stellar radius. Indeed, the Roche lobe radius is far more appropriate to describe the size of the companion (e.g., Stappers et al. 1996; Pallanca et al. 2012, 2014a; Breton et al. 2013). According to Eggleton (1983), the Roche lobe radius can be computed as:

$$\frac{R_{\text{RL}}}{a} \simeq \frac{0.49q^{\frac{2}{3}}}{0.6q^{\frac{2}{3}} + \ln\left(1 + q^{\frac{1}{3}}\right)}, \quad (1)$$

where q is the ratio between the companion and the PSR masses and a is the orbital separation. Combining this relation with the PSR mass function, assuming an NS mass ranging from $1.2 M_{\odot}$ to $2.5 M_{\odot}$ (Özel et al. 2012) and an inclination angle ranging from 0° to 90° , we find $0.22 R_{\odot} < R_{\text{RL}} < 1.24 R_{\odot}$.

Interestingly, the shape of the light curve presents a hint of asymmetric structure in both filters: the increase to the maximum seems to be smoother than the decrease to the minimum. Despite the low statistic, this behavior could be due to a slightly asynchronous rotating companion, as in the case of PSR J2051–0827 (see Stappers et al. 2001). This could be the result of a tidal torque from the wind of a magnetically active star, which can result in an angular velocity of the companion that differs from the orbital angular velocity. Moreover, in this case the angular velocity could be subject to a variation with time due to a secular time dependence of the orbital period, due itself to a variation of the companion’s quadrupole moment (see e.g., Applegate & Shaham 1994; Doroshenko et al. 2001; Lorimer & Kramer 2012). However, in order to probe this intriguing possibility, a uniform sampling of the light curve from new observations is needed.

4.1. Reprocessing Efficiency and Roche Lobe Filling Factor

Under the assumption that the optical magnitude modulation is mainly due to the heating of the companion surface by the

¹⁴ <http://basti.oa-teramo.inaf.it>

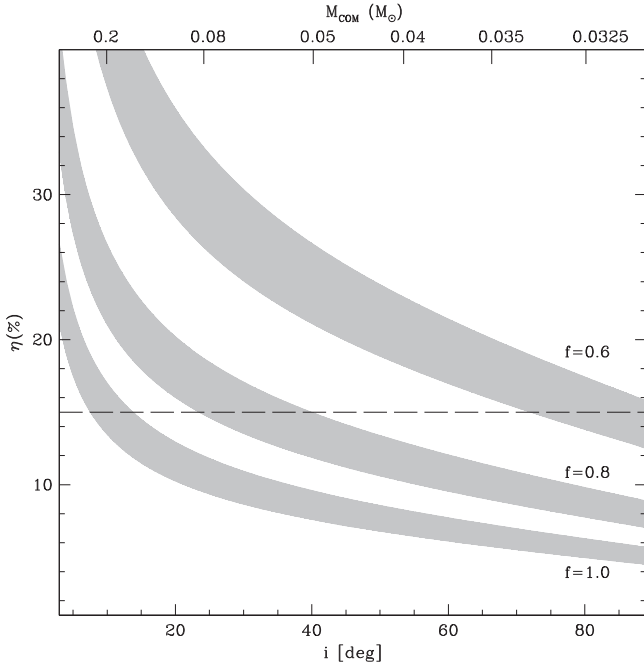


Figure 8. Reprocessing efficiency of the PSR emitted energy as a function of the inclination angle, assuming three different values of the Roche lobe filling factor and a PSR mass of $1.4 M_{\odot}$. The thickness of each strip corresponds to the range of spin-down energies measured for this PSR (see text). The horizontal dashed line at $\eta = 15\%$ is a typical reprocessing efficiency reported in Breton et al. (2013). On the top axis, the companion masses for a PSR mass of $1.4 M_{\odot}$ are reported.

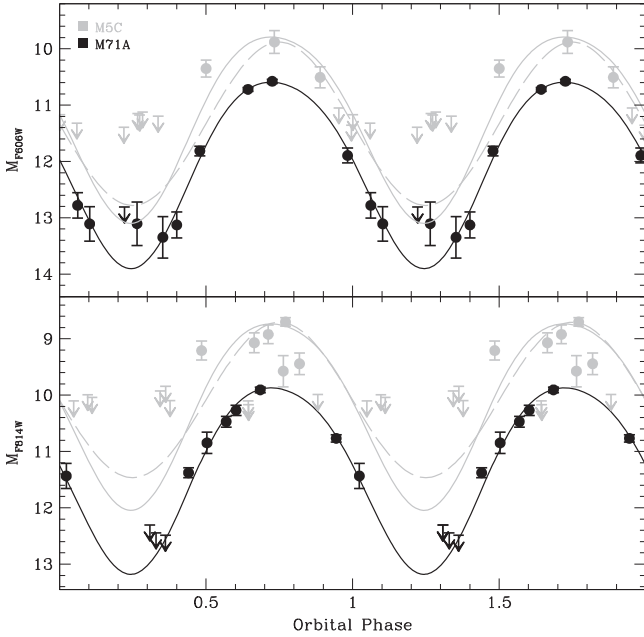


Figure 9. Optical light curves of COM-M71A (this work; black points and lines) and COM-M5C (from Pallanca et al. 2014a; gray points and dashed lines), with magnitudes reported as absolute values. The gray solid lines show the COM-M71A model adapted to COM-M5C to reproduce the observed points.

PSR flux, we can compare the observed flux amplitude of the light curve with the expected one (ΔF_{exp}) as a function of the inclination angle i using the following relation (Pallanca et al.

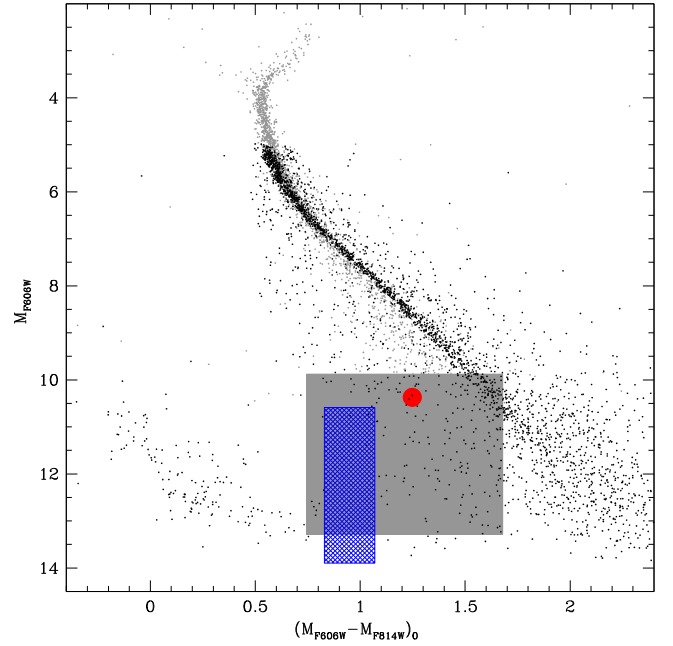


Figure 10. CMD of M71 (black dots) and M5 (gray dots). The blue shaded region is the position of COM-M71A along the whole orbital phase, as derived from the light-curve model (see Figure 7). The red point and the gray area are the indicative position of COM-M5C (see Pallanca et al. 2014a, for more details). Both the objects are located between the MS and the WD cooling sequence, suggesting common properties of these two BW companions.

2014a):

$$\Delta F_{\text{exp}}(i) = \eta \frac{\dot{E}}{a^2} R_{\text{COM}}^2(i) \frac{\epsilon(i)}{4\pi d_{\text{PSR}}^2}, \quad (2)$$

where η is the reprocessing efficiency under the assumption of isotropic emission from the PSR, $R_{\text{COM}}(i) = fR_{\text{RL}}(i)$ is the companion star's radius, where f is the volume-averaged Roche lobe filling factor, d_{PSR} is the MSP distance, assumed to be equal to the GC distance ($d_{\text{PSR}} = 4.0$ kpc; Harris 1996), and $\epsilon(i)$ parameterizes the difference in the heated surface visible to the observer between maximum and minimum, as a function of the inclination angle. $\dot{E} = 4\pi I \frac{\dot{P}}{P^3}$ is the PSR spin-down luminosity where I is the moment of inertia. Using the spin period and its intrinsic first derivative obtained from radio timing (Table 1) and assuming $I = 10^{45}$ g cm², we found that $4.6 \cdot 10^{33}$ ergs s⁻¹ $< \dot{E} < 5.8 \cdot 10^{33}$ ergs s⁻¹, typical values within the Galactic eclipsing MSP population. Setting $\Delta F_{\text{exp}} = \Delta F_{\text{obs}}$ in the F606W filter (see Table 3), we evaluated the reprocessing efficiency as a function of the inclination angle for different values of the Roche lobe filling factor. Results are shown in Figure 8. As can be seen, for high inclination angles and a Roche lobe-filling companion, the reprocessing efficiency is $\sim 5\%$, while for filling factor $f = 0.8$ it is $\sim 8\%$. A typical value of 15% (Breton et al. 2013) would be consistent with $f \sim 0.6$. Values of $f < 1$ would be plausible since some works show that BW companions do not always completely fill their Roche lobe (e.g., Callanan et al. 1995; Stappers et al. 1999; Breton et al. 2013). Similar results hold for the F814W filter.

It is worth noting that by using R_{BB} instead of R_{RL} for the stellar radius, the efficiency increases over 100% for almost every meaningful configuration. This can be admitted only if

anisotropic PSR emission is assumed. However, the presence of long radio eclipses and the behavior of similar objects is a strong indication that R_{BB} heavily underestimates the true stellar radius.

4.2. A Comparison between M71A and M5C

So far, the optical companion to PSR J1518+0204C (hereafter M5C) was the only BW companion known in a GC. M5C is a 2.48 ms PSR with an orbital period of ~ 2.1 hr located in the GC M5. Its radio timing and the optical photometry of the companion star (COM-M5C) are discussed in Pallanca et al. (2014a). In Section 3, we anticipated some interesting analogies between this star and COM-M71A. In order to further investigate similarities between these BW companions, we compared the optical properties of the two objects. Figure 9 shows their light curves, with the magnitudes reported as the absolute values. Indeed, despite the low sampling of the COM-M5C light curves, these two objects seem to have a quite similar optical behavior. As a reference, we used COM-M71A analytical models (solid lines) for the COM-M5C, from which we inferred that a similar light curve structure could hold even for COM-M5C, being more appropriate than the simple sinusoid (dashed lines) used by Pallanca et al. (2014a), given the sparse number of measurements that prevent them from building an accurate model. Figure 10 shows the position of the two objects in the CMD. Again, considering the uncertainties in COM-M5C magnitudes and colors, we found that they are located in the same region, suggesting a common evolutionary path for these low-mass, possibly nondegenerate, swollen, and heated companions. Interestingly, in the CMD the two BW companions are located in a region completely different from that usually occupied by RBs (Pallanca 2014b). Of course, additional identifications of BW companions are needed to firmly characterize the evolution of these objects. In addition, using Equation (2) for COM-M5C, setting the filling factor $f = 1$, and using the spin-down period from Pallanca et al. (2014a) to evaluate the spin-down luminosity ($0.7 \cdot 10^{34} \text{ erg s}^{-1} < \dot{E}_{\text{M5C}} < 3 \cdot 10^{34} \text{ erg s}^{-1}$), we found a reprocessing efficiency $\eta \sim 5\% - 20\%$, a value fully in agreement with that found for COM-M71A, thus further strengthening the analogies between these two systems.

4.3. Comparing X-ray and Optical Light Curves

Usually, BWs with a high-energy counterpart do not show any appreciable X-ray variability related to their orbital period (see, e.g., Bogdanov et al. 2006; Gentile et al. 2014, respectively for the BWs in the GC 47 Tucanae and in the Galactic field). However, this could be an observational bias, due to the lack of deep enough and systematic surveys of BWs in X-rays. On the other hand, it is worth noting that several RB systems clearly show orbital X-ray modulation likely due to the presence of intra-binary shocks (Bogdanov et al. 2006, 2011, 2014). M71A is an exception, since it has been found to show periodic X-ray variability (Elsner et al. 2008). Very interestingly, the determination of COM-M71A's optical light curve offers the opportunity to perform a comparison between the two. The most intriguing feature emerging from the comparison of the light curves (both folded with the binary system parameters) is that the phase spanned by the radio eclipses ($0.18 < \phi < 0.35$) does not correspond to the phase of the X-ray minimum ($0 < \phi < 0.2$), but it nicely lines up

with the optical minimum ($\phi \approx 0.25$). Thus we found that the X-ray minimum precedes the superior conjunction of the optical PSR. A similar effect was already observed for the RB 47TucW, a 2.35 ms binary MSP with an orbital period of ~ 3.2 hr and a companion mass of $\sim 0.15 M_{\odot}$ (Camilo et al. 2000), whose optical light curves indicate the presence of a strong heating (Edmonds et al. 2002), as usually observed for BW systems. For this object Bogdanov et al. (2006) argue that the X-ray variability can be attributed to the presence of an intra-binary shock that is eclipsed by the companion star. The length of the X-ray eclipse suggests that this shock is located closer to the companion star than to the MSP. In particular, this behavior could be due to a swept-back shocked region, produced by the interaction between the PSR wind and the stream of gas issuing from the inner Lagrange point L1, elongated perpendicular to the semimajor axis of the binary (see Bogdanov et al. 2005, for a detailed description). Despite the low X-ray statistics, this is likely to be the case also for M71A, where the intra-binary shock could be eclipsed just before the PSR superior conjunction. Even for a companion that is underfilling its Roche lobe, this shocked region can be created thanks to the stellar wind, which can result in mass outflow through L1 (Bogdanov et al. 2005).

As discussed in Bogdanov et al. (2005), the Accreting Millisecond X-ray Pulsar (AMXP) SAX J1808.4–3658, during quiescent states, shows several analogies with RB 47TucW, in terms of both the X-ray spectrum and the optical variability. Based on the discussion above, these properties are also similar to those observed for M71A and, very interestingly, even the companion mass is comparable in these two cases: above $0.032 M_{\odot}$ for COM-M71A, and $\sim 0.05 M_{\odot}$ for the companion to SAX J1808.4–365 (Campana et al. 2004). This puts M71A in the middle of the riddle, supporting the possibility that AMXPs could be the bridge between RB and BW systems (Roberts et al. 2014). Clearly, multi-wavelength studies of these objects are urged to unveil connections between AMXPs and eclipsing MSPs, and between BWs and RBs. Indeed, several important new connections between AMXPs and RBs have been made in the last years, especially with the discoveries of systems transitioning from one state to the other (see Archibald et al. 2009; Papitto et al. 2013; Bassa et al. 2014; Patruno et al. 2014; Stappers et al. 2014).

5. SUMMARY AND CONCLUSION

We presented a phase-connected radio timing solution for the BW PSR J1953+1846 A, which includes a very precise determination of position and orbital parameters. Taking advantage of this precise measurement of the PSR position, we have used a set of high-resolution ACS/HST images to search for the companion star in the optical bands. We identified a faint and strongly variable star (COM-M71A), showing a modulation of at least three magnitudes in both filters used (F606W and F814W). In the CMD, COM-M71A lies in the region between the cluster MS and the WD cooling sequences, thus suggesting that it is a low-mass, nondegenerate or at least semi-degenerate star, with a temperature of about 5100 K. Unfortunately, because of its faintness, it was detectable only in 16 out of 27 images, mostly during the PSR inferior conjunction. The light curve shows a sinusoidal shape with a period fully consistent with the binary MSP. The maximum, during the PSR inferior conjunction, and the minimum, during the PSR superior conjunction, suggest a

strong heating of the side of the companion star exposed to the PSR flux. Such a behavior is in good agreement with that observed for similar objects in the Galactic field. By modeling the light curve, we showed that the companion's reprocessing efficiency of the PSR energy is $\sim 5\%$ for a Roche lobe-filling companion, while a typical value of 15% is reasonable by assuming a filling factor of 0.6. The comparison between the optical and X-ray light curves suggests the possible presence of intra-binary shocks, similarly to what is observed for RB 47TucW. An X-ray and optical follow-up will highlight the presence of these shocks and possibly will allow us to characterize their properties and structure. Unfortunately, the star is too faint to allow a spectroscopic follow-up with the available instruments. However, an optimized photometric follow-up would provide the opportunity to better constrain the system properties, and by using, for example, phase-resolved observations with a narrow H α filter we could constrain the presence of ionized material, eventually related to the intra-binary shocks.

COM-M71A is, so far, the second BW optical companion identified in a GC after COM-M5C in M5. Interestingly, both the shape of the light curve and the position in the CMD are quite similar in the two systems. This suggests that probably the two objects undergo a similar evolutionary path. Even though the statistic is far too limited to draw any meaningful conclusion, at the moment there is no evidence for any significant difference from the BW optical companions observed in the field, probably suggesting that no dynamical interactions are strictly needed to form these systems.

This research is part of the project *Cosmic-Lab* (<http://www.cosmic-lab.eu>) funded by the European Research Council under contract ERC-2010-AdG-267675. J.W.T.H. acknowledges funding from an NWO Vidi fellowship and ERC starting grant "DRAGNET" (337062).

REFERENCES

- Alpar, M. A., Cheng, A. F., Ruderman, M. A., & Shaham, J. 1982, *Natur*, **300**, 728
- Anderson, J., Sarajedini, A., Bedin, L. R., et al. 2008, *AJ*, **135**, 2055
- Applegate, J. H., & Shaham, J. 1994, *ApJ*, **436**, 312
- Archibald, A. M., Kaspi, V. M., Hessels, J. W. T., et al. 2013, arXiv:1311.5161
- Archibald, A. M., Stairs, I. H., Ransom, S. M., et al. 2009, *Sci*, **324**, 1411
- Arzoumanian, Z., Fruchter, A. S., & Taylor, J. H. 1994, *ApJL*, **426**, L85
- Bailyn, C. D. 1992, *ApJ*, **392**, 519
- Bassa, C. G., Patruno, A., Hessels, J. W. T., et al. 2014, *MNRAS*, **441**, 1825
- Bates, S. D., Bailes, M., Bhat, N. D. R., et al. 2011, *MNRAS*, **416**, 2455
- Benvenuto, O. G., De Vito, M. A., & Horvath, J. E. 2014, *ApJL*, **786**, LL7
- Bhattacharya, D., & van den Heuvel, E. P. J. 1991, *PhR*, **203**, 1
- Blandford, R., & Teukolsky, S. A. 1976, *ApJ*, **205**, 580
- Bogdanov, S., Archibald, A. M., Hessels, J. W. T., et al. 2011, *ApJ*, **742**, 97
- Bogdanov, S., Grindlay, J. E., Heinke, C. O., et al. 2006, *ApJ*, **646**, 1104
- Bogdanov, S., Grindlay, J. E., & van den Berg, M. 2005, *ApJ*, **630**, 1029
- Bogdanov, S., Patruno, A., Archibald, A. M., et al. 2014, *ApJ*, **789**, 40
- Bohlin, R. C. 2012, Instrument Science Rep. ACS 2012-01
- Burgay, M., Joshi, B. C., D'Amico, N., et al. 2006, *MNRAS*, **368**, 283
- Breton, R. P., van Kerkwijk, M. H., Roberts, M. S. E., et al. 2013, *ApJ*, **769**, 108
- Callanan, P. J., van Paradijs, J., & Rengelink, R. 1995, *ApJ*, **439**, 928
- Camilo, F., Lorimer, D. R., Freire, P., Lyne, A. G., & Manchester, R. N. 2000, *ApJ*, **535**, 975
- Campana, S., D'Avanzo, P., Casares, J., et al. 2004, *ApJL*, **614**, L49
- Chen, H.-L., Chen, X., Tauris, T. M., & Han, Z. 2013, *ApJ*, **775**, 27
- Cocozza, G., Ferraro, F. R., Possenti, A., et al. 2008, *ApJL*, **679**, L105
- Cool, A. M., Grindlay, J. E., Cohn, H. N., Lugger, P. M., & Slavin, S. D. 1995, *ApJ*, **439**, 695
- Dalessandro, E., Lanzoni, B., Ferraro, F. R., et al. 2008a, *ApJ*, **677**, 1069
- Dalessandro, E., Lanzoni, B., Ferraro, F. R., et al. 2008b, *ApJ*, **681**, 311
- Doroshenko, O., Löhmer, O., Kramer, M., et al. 2001, *A&A*, **379**, 579
- Dowd, A., Sisk, W., & Hagen, J. 2000, in IAU Colloq. 177, Pulsar Astronomy —2000 and Beyond, ed. M. Kramer, N. Wex, & R. Wielebinski (San Francisco, CA: ASP), 275
- Edmonds, P. D., Gilliland, R. L., Camilo, F., Heinke, C. O., & Grindlay, J. E. 2002, *ApJ*, **579**, 741
- Edmonds, P. D., Gilliland, R. L., Heinke, C. O., Grindlay, J. E., & Camilo, F. 2001, *ApJL*, **557**, L57
- Eggleton, P. P. 1983, *ApJ*, **268**, 368
- Eichler, D., & Levinson, A. 1988, *ApJL*, **335**, L67
- Elsner, R. F., Heinke, C. O., Cohn, H. N., et al. 2008, *ApJ*, **687**, 1019
- Ferraro, F. R., Clementini, G., Fusi Pecci, F., & Buonanno, R. 1991, *MNRAS*, **252**, 357
- Ferraro, F. R., Clementini, G., Fusi Pecci, F., Sortino, R., & Buonanno, R. 1992, *MNRAS*, **256**, 391
- Ferraro, F. R., D'Amico, N., Possenti, A., Mignani, R. P., & Paltrinieri, B. 2001b, *ApJ*, **561**, 337
- Ferraro, F. R., Dalessandro, E., Mucciarelli, A., et al. 2009, *Natur*, **462**, 483
- Ferraro, F. R., Fusi Pecci, F., & Bellazzini, M. 1995, *A&A*, **294**, 80
- Ferraro, F. R., Lanzoni, B., Dalessandro, E., et al. 2012, *Natur*, **492**, 393
- Ferraro, F. R., Possenti, A., D'Amico, N., & Sabbi, E. 2001a, *ApJL*, **561**, L93
- Ferraro, F. R., Possenti, A., Sabbi, E., & D'Amico, N. 2003a, *ApJL*, **596**, L211
- Ferraro, F. R., Possenti, A., Sabbi, E., et al. 2003b, *ApJ*, **595**, 179
- Ferraro, F. R., Sabbi, E., Gratton, R., et al. 2003c, *ApJL*, **584**, L13
- Freire, P. C. C., Hessels, J. W. T., Nice, D. J., et al. 2005, *ApJ*, **621**, 959
- Fruchter, A. S., Stinebring, D. R., & Taylor, J. H. 1988, *Natur*, **333**, 237
- Geffert, M., & Maintz, G. 2000, *A&AS*, **144**, 227
- Gentile, P. A., Roberts, M. S. E., McLaughlin, M. A., et al. 2014, *ApJ*, **783**, 69
- Goldsbury, R., Richer, H. B., Anderson, J., et al. 2010, *AJ*, **140**, 1830
- Goldsbury, R., Richer, H. B., Anderson, J., et al. 2011, *AJ*, **142**, 66 Erratum
- Goodman, J., & Hut, P. 1989, *Natur*, **339**, 40
- Hack, W., & Cox, C. 2001, Instrument Science Rep. ACS 2001-008
- Harris, W. E. 1996, *AJ*, **112**, 1487
- Hessels, J. W. T., Ransom, S. M., Stairs, I. H., Kaspi, V. M., & Freire, P. C. C. 2007, *ApJ*, **670**, 363
- Huang, R. H. H., Becker, W., Edmonds, P. D., et al. 2010, *A&A*, **513**, A16
- Hut, P., McMillan, S., Goodman, J., et al. 1992, *PASP*, **104**, 981
- Ivanova, N., Heinke, C. O., Rasio, F. A., Belczynski, K., & Fregeau, J. M. 2008, *MNRAS*, **386**, 553
- Keith, M. J., Johnston, S., Bailes, M., et al. 2012, *MNRAS*, **419**, 1752
- Keith, M. J., Johnston, S., Ray, P. S., et al. 2011, *MNRAS*, **414**, 1292
- Kharchenko, N. V., Piskunov, A. E., Schilbach, E., Röser, S., & Scholz, R.-D. 2013, *A&A*, **558**, AA53
- King, A. R., Davies, M. B., & Beer, M. E. 2003, *MNRAS*, **345**, 678
- Li, M., Halpern, J. P., & Thorstensen, J. R. 2014, *ApJ*, **795**, 115
- Lorimer, D. R., & Kramer, M. 2012, in Handbook of Pulsar Astronomy (Cambridge, UK: Cambridge Univ. Press)
- Manzot, P., Pietrinferni, A., Gasparo, F., Taffoni, G., & Cordier, D. 2008, *PASP*, **120**, 922
- Meurer, G. R., Lindler, D., Blakeslee, J. P., et al. 2003, in *HST* Calibration Workshop: Hubble After the Installation of the ACS and the NICMOS Cooling System, ed. S. Arribas, A. Koekemoer, & B. Whitmore (Baltimore, MD: STScI), 65
- Moffat, A. F. J. 1969, *A&A*, **3**, 455
- Mucciarelli, A., Salaris, M., Lanzoni, B., et al. 2013, *ApJL*, **772**, L27
- Ng, C., Bailes, M., Bates, S. D., et al. 2014, *MNRAS*, **439**, 1865
- Nice, D. J., & Taylor, J. H. 1995, *ApJ*, **441**, 429
- Özel, F., Psaltis, D., Narayan, R., & Santos Villarreal, A. 2012, *ApJ*, **757**, 55
- Pallanca, C. 2014, arXiv:1405.2898
- Pallanca, C., Dalessandro, E., Ferraro, F. R., et al. 2010, *ApJ*, **725**, 1165
- Pallanca, C., Dalessandro, E., Ferraro, F. R., Lanzoni, B., & Beccari, G. 2013, *ApJ*, **773**, 122
- Pallanca, C., Mignani, R. P., Dalessandro, E., et al. 2012, *ApJ*, **755**, 180
- Pallanca, C., Ransom, S. M., Ferraro, F. R., et al. 2014, *ApJ*, **795**, 29
- Papitto, A., Ferrigno, C., Bozzo, E., et al. 2013, *Natur*, **501**, 517
- Patruno, A., Archibald, A. M., Hessels, J. W. T., et al. 2014, *ApJL*, **781**, LL3
- Phinney, E. S. 1992, *RSPTA*, **341**, 39
- Pooley, D., Lewin, W. H. G., Anderson, S. F., et al. 2003, *ApJL*, **591**, L131
- Possenti, A., D'Amico, N., Manchester, R. N., et al. 2003, *ApJ*, **599**, 475
- Ransom, S., Hessels, J., Stairs, I., et al. 2005b, Binary Radio Pulsars, **328**, 199
- Ransom, S. M., Hessels, J. W. T., Stairs, I. H., et al. 2005a, *Sci*, **307**, 892
- Ransom, S. M., Ray, P. S., Camilo, F., et al. 2011, *ApJL*, **727**, LL16

- Reid, M. J., Menten, K. M., Brunthaler, A., et al. 2014, *ApJ*, **783**, 130
- Reynolds, M. T., Callanan, P. J., Fruchter, A. S., et al. 2007, *MNRAS*, **379**, 1117
- Roberts, M. S. E., McLaughlin, M. A., Gentile, P., et al. 2014, *AN*, **335**, 313
- Ruderman, M., Shaham, J., Tavani, M., & Eichler, D. 1989, *ApJ*, **343**, 292
- Sabbi, E., Gratton, R. G., Bragaglia, A., et al. 2003a, *A&A*, **412**, 829
- Sabbi, E., Gratton, R., Ferraro, F. R., et al. 2003b, *ApJL*, **589**, L41
- Salaris, M., Cassisi, S., Pietrinferni, A., Kowalski, P. M., & Isern, J. 2010, *ApJ*, **716**, 1241
- Shklovskii, I. S. 1970, *SvA*, **13**, 562
- Sigurdsson, S., Richer, H. B., Hansen, B. M., Stairs, I. H., & Thorsett, S. E. 2003, *Sci*, **301**, 193
- Stappers, B. W., Archibald, A. M., Hessels, J. W. T., et al. 2014, *ApJ*, **790**, 39
- Stappers, B. W., Bessell, M. S., & Bailes, M. 1996, *ApJL*, **473**, L119
- Stappers, B. W., van Kerkwijk, M. H., Bell, J. F., & Kulkarni, S. R. 2001, *ApJL*, **548**, L183
- Stappers, B. W., van Kerkwijk, M. H., Lane, B., & Kulkarni, S. R. 1999, *ApJL*, **510**, L45
- Stetson, P. B. 1987, *PASP*, **99**, 191
- Taylor, J. H. 1992, *Phil. Trans. Roy. Soc. A*, **341**, 117
- Verbunt, F., & Freire, P. C. C. 2014, *A&A*, **561**, AA11